

A Survey of Star Clusters in the M31 Southwest Field. *UBVRI* Photometry and Multiband Maps

D. Narbutis¹, V. Vansevičius¹, K. Kodaira², A. Bridžius¹, and R. Stonkutė¹

ABSTRACT

A new survey of star clusters in the southwest field of the M31 disk based on the high resolution Subaru Suprime-Cam observations is presented. The *UBVRI* aperture CCD photometry catalog of 285 objects ($V \lesssim 20.5$ mag; 169 of them identified for the first time) is provided. Each object is supplemented with multiband color maps presented in the electronic edition of the *Astrophysical Journal Supplement*. Seventy seven star cluster candidates from the catalog are located in the *Hubble Space Telescope* archive frames.

Subject headings: galaxies: individual (M31) — galaxies: star clusters

1. Introduction

Detailed studies of the star clusters in M31 are essential to understanding the evolution mechanisms of disk galaxies and of the cluster population itself. Many observational surveys of this galaxy have been devoted to globular clusters; see, e.g., Kim et al. (2007) and references therein. Due to crowding, plausible detection and analysis of star clusters projected on the disk of M31 became feasible only with high-resolution imaging; see Krienke & Hodge (2007) for an extensive discussion of the problem. However, *Hubble Space Telescope* (*HST*) observations cover only a small part of the M31 disk, and up-to-date cluster population studies (e.g., Krienke & Hodge 2007) are based on *HST* fields scattered over the area of M31.

A homogeneous (in object detection and photometry) survey of star clusters in the southwest field of the M31 disk was conducted by Kodaira et al. (2004) (hereafter Paper I) over an area of ~ 500 arcmin², making use of the high-resolution imaging capability of

¹Institute of Physics, Savanorių 231, Vilnius LT-02300, Lithuania, wladas@astro.lt

²The Graduate University for Advanced Studies (SOKENDAI), Shonan Village, Hayama, Kanagawa 240-0193, Japan

the Subaru Suprime-Cam (Miyazaki et al. 2002). In Paper I we presented a catalog of 49 prominent compact objects and a catalog of 52 emission objects. Structural parameters of 49 compact and 2 emission objects brighter than $V \sim 19.0$ mag were derived from the V -band Suprime-Cam image by Šablevičiūtė et al. (2006, 2007), showing that they are fainter and span a slightly wider half-light radius range than the M31 clusters studied by Barmby et al. (2002, 2007). The $UBVRI$ (R and I bands are in Cousins system) photometry of these clusters was performed on the Local Group Galaxy Survey (LGGS; Massey et al. 2006) images by Narbutis et al. (2006), resulting in a smaller scatter in color-color diagrams than photometry data of the same objects taken from the Revised Bologna Catalogue of M31 globular clusters and candidates compiled by Galletti et al. (2004).

Promising results from these studies motivated us to extend a sample of star clusters up to $V \sim 20.5$ mag. Here we present the results of $UBVRI$ aperture CCD photometry for 285 star cluster candidates located in the same Suprime-Cam field of the M31 disk (see Figure 1). The multiband color maps, combined from *GALEX*, LGGS, 2MASS, *Spitzer* (24 μm), and HI (21 cm) images, are provided in the electronic edition of the *Supplement*.

We describe the object selection procedure in section 2, photometry and calibration in section 3, and present the catalog in section 4.

2. Object Selection

The Suprime-Cam survey of star cluster-like objects was conducted in the southwest (SW) field of the M31 disk ($\sim 17.5 \times 28.5$ in size), centered at $\alpha_{\text{J}2000} = 0^{\text{h}}40^{\text{m}}9$ and $\delta_{\text{J}2000} = +40^{\circ}45'$ (Figure 1). Visual inspection of the high-resolution Suprime-Cam mosaic images, with characteristic full width at half-maximum (FWHM) of the point-spread function (PSF) of $\sim 0.7''$, enabled us to select the initial sample of ~ 600 star cluster candidates up to $V \sim 21^{\text{m}}$.

In addition, several objects that were not recognized as cluster candidates in our survey, were appended to the initial Suprime-Cam object sample from the Revised Bologna Catalogue of M31 globular clusters and candidates v.3.2, July 2007¹ (Galletti et al. 2007) and from the recent *HST* survey of the M31 disk cluster population conducted by Krienke & Hodge (2007). About 40 objects, included in Galletti et al. (2007) and overlapping with our survey field originally come from the recent survey by Kim et al. (2007), however, $\sim 50\%$ of these objects were omitted from our catalog because their surface brightness profiles closely

¹See <http://www.bo.astro.it/M31/>.

resemble that of stars.

To study selection effects inherent to the initial cluster candidate sample, archival *HST* frames (see Appendix A) were employed. A completeness of $\sim 70\%$ in the visual selection of star cluster candidates at the limiting magnitude of the catalogue ($V \sim 20.5$ mag) was estimated by comparing our initial sample of ~ 600 objects with an overlapping sample studied by Krienke & Hodge (2007). We also checked our objects against available archival *HST* images, and some of our cluster candidates were classified as asterisms. Moreover, few new star cluster candidates, overlooked during a visual inspection of the Suprime-Cam images, were found on *HST* frames. Summing up results of these tests, we find the completeness of our cluster candidate sample to be higher than $\sim 50\%$ at $V = 20.5$ mag. This is a conservative magnitude limit for objects that can be identified as star clusters on the Suprime-Cam images. However, it is difficult to estimate the completeness of the present cluster candidate sample more accurately, since it depends on a strongly varying background object density across the surveyed area, and the clusters' luminosities, colors, and concentrations.

A strong contamination of young star cluster samples selected in M31 by asterisms has been demonstrated recently by Cohen et al. (2005). Therefore, in order to clean our cluster candidate sample ($V \lesssim 20.5$ mag), we determined cluster structural parameters, by employing the BAOLAB/ISHAPE program package (Larsen 1999) and using the analysis technique described in Šablevičiūtė et al. (2006). Unresolved objects with determined intrinsic sizes of $\lesssim 0.2''$ have been removed as suspected stars. The analysis of multiband color maps and ISHAPE results revealed several red objects, possessing smooth elliptical surface brightness distributions. They were also removed from the sample as probable background galaxies. We did not include KWC13 and KWC24 from Paper I either, suspecting them to be background galaxies. After performing this cleaning, we ended up with the final catalog containing 285 star cluster candidates (169 of them identified for the first time). The final cluster candidate sample includes 77 objects observed by *HST*.

3. Photometry

For the star cluster aperture photometry, we used LGGS² U , B , V , R , and I band mosaic images of four M31 fields (F6, F7, F8, and F9) overlapping with the field studied in Paper I. The mosaic camera used for LGGS consists of eight CCDs. Each CCD chip covers a $9' \times 18'$ field and has an individual set of color equations. The observations and data reductions are described in detail by Massey et al. (2006).

²LGGS: <http://www.lowell.edu/users/massey/lgsurvey.html>.

We considered mosaic images, cleaned of cosmic rays and cosmetic defects, to be preferable to individual exposure images for star cluster aperture photometry. The dithering pattern of five individual exposures is the same for each field (maximum shifts up to $1'$ from the first exposure), with an exception of the U -band mosaic of the F9 field, which is combined of from six individual exposures. Massey et al. (2006) do not recommend a straightforward use of their mosaic images for accurate photometry, therefore, we treated each CCD chip area in the mosaic image separately, taking special care of objects residing in different CCDs of the combined individual exposures.

3.1. PSF homogenization

PSFs of the LGGS mosaic images used for aperture photometry differ significantly (see Table 1). Moreover, four of them have a coordinate-dependent PSF with a FWHM varying by more than $0.2''$ across the field. That would lead to a variable aperture correction and, if not properly corrected, to a cluster color bias for the small apertures (diameter of $\sim 3''$) used in this study. Since the intrinsic surface brightness distribution profiles of star cluster candidates are unknown, we homogenized mosaic image PSF shapes, instead of using variable aperture corrections. This also ensures a consistency in aperture selection, photometric error and photometric background estimates.

We applied the DAOPHOT package (Stetson 1987) from the IRAF program system (Tody 1993) to compute original PSFs for all mosaic images. By convolving the widest PSF ($\text{FWHM} = 1.3''$) with the Gaussian kernel, a reference PSF of $\text{FWHM} = 1''.5$ was produced. The IRAF's `psfmatch` procedure was employed to compute the required convolution kernels for individual mosaic images with respect to the reference PSF. These kernels were symmetrized by replacing their cores with the best-fitting Gaussian profiles, and their wings with the best-fitting exponential profiles, truncated at $3.5''$. The IRAF's `convolve` procedure was employed to produce mosaic images possessing unique and coordinate-independent PSFs of $\text{FWHM} = 1.5''$. The homogenized images were photometrically calibrated and used for star cluster photometry. The maximum difference of the aperture corrections in different pass-bands is less than 0.02 mag. A test of photometric accuracy of the entire PSF homogenization procedure suggests that errors do not exceed 0.01 mag.

3.2. Calibrations

For the *UBVRI* cluster photometry calibration we selected well-isolated stars of high photometric accuracy (<0.03 mag), measured in each pass-band more than 3 times, from Table 4 of Massey et al. (2006). The calibration stars were measured on the homogenized mosaic images through the circular aperture of $3.0''$ in diameter by employing the IRAF’s `phot` procedure. The aperture correction (aperture magnitude minus total magnitude) of 0.27 mag was determined for all homogenized mosaic images.

Massey et al. (2006) provide color equations for individual CCD chips of the mosaic camera (see their Table 2). We solved those equations by fitting photometric zero-points of all pass-bands for every individual field and CCD chip. Typically, 80 (ranging from 20 to 140) calibration stars per chip were used. The final errors of derived zero-points are less than 0.01 mag with typical fitting rms < 0.03 mag for the *I* band and < 0.02 mag for other pass-bands. Color equations given by Massey et al. (2006), supplemented with the derived zero-points, were used to transform instrumental magnitudes to the standard system. For objects located in the mosaic image areas combined from different CCDs, we used color equations of corresponding CCDs and performed independent transformations to the standard system.

A comparison of three published stellar photometry data sets in the SW field of the M31 disk (Narbutis, Stonkutė & Vansevičius 2006) suggests caution when using tertiary standards as local photometric standards. However, a careful reduction, calibration, and internal consistency check performed by Massey et al. (2006) resulted in millimagnitude differences between the photometry results of overlapping fields. To our knowledge, this is the most accurately calibrated photometry data set in the M31 galaxy to date.

3.3. Results

The aperture *UBVRI* photometry was carried out by employing the IRAF’s XGPHOT package. The images of all objects, except for five saturated in the *I* band, are free of visible defects. Apertures were centered on clusters’ luminosity distribution peaks in the Suprime-Cam *V*-band mosaic image and transformed to individual LGGS image coordinate systems with the IRAF’s `geoxytran` procedure. In order to minimize cluster photometry contamination by background objects in crowded fields, we decided to use individual small circular (elliptical for the two bright objects KW102 and KW141 to avoid obvious nearby background stars) apertures; their sizes are provided in Table 2. The photometric background was determined in individually selected and object-centered circular annuli with typical inner and outer radii of $3''$ and $8''$, respectively. For some clusters, located on a largely

variable background, circular background determination zones were selected individually in representative areas.

The catalog of 285 star cluster candidates consists of 138 and 141 objects measured in two and three different LGGS fields, respectively, while six objects have been measured in one field. Two main types of error sources determine the final accuracy of the photometry: the photon noise – σ_n (estimated by XGPHOT) and the calibration procedure – σ_c . The V -band magnitude and colors, derived in different LGGS fields for each object, were examined interactively. Weighted averages were calculated taking into account individual σ_n and down-weighting data derived in the mosaic image areas combined from different CCDs. The rms of averaged magnitudes and colors characterize calibration errors in general, therefore, they were assigned to σ_c . The lowest possible calibration errors of 0.010, 0.015, 0.020 mag were set for objects having 3, 2, and 1 independent measurements, respectively. The final photometric errors, provided in the catalog (Table 2), are calculated as $\sigma = (\sigma_n^2 + \sigma_c^2)^{1/2}$. The photometric error values, σ_V , for corresponding V -band magnitudes are plotted in Figure 2.

In order to check the aperture size effect on the color accuracy and possible bias due to a contamination by background stars, all objects were measured through four additional apertures, changing the adopted size by $\pm 0.6''$ and $\pm 1.2''$. The results of the aperture size test, published by Narbutis et al. (2007), show that contaminating background stars have the strongest influence in I band. The $U - B$ color of red objects tends to be systematically bluer, and an opposite effect is observed for the $V - I$ of blue objects. However, in most cases the final photometric errors provided in the catalog (Table 2) represent the accuracy of cluster colors well. A comparison of our photometry data with *HST* observations of the same objects by Krienke & Hodge (2007) shows a reasonably good agreement (Narbutis et al. 2007).

4. The Catalog

The photometric catalog of 285 star cluster candidates in the SW M31 field is presented in Table 2. Object coordinates, V -band aperture magnitudes, $U - B$, $B - V$, $V - R$, and $R - I$ colors with their photometric errors, a flag for 77 objects located in *HST* frames, and cross-identifications with Galleti et al. (2007), Krienke & Hodge (2007), and Paper I (69, 24, and 58 clusters, respectively) are provided.

All catalog objects, overlaid on the *Spitzer* 24 μm image, are shown in Figure 1. Elliptical ring segments, indicating distances (6 – 18 kpc) from the M31 center in the galaxy’s disk plane, were drawn assuming the following M31 parameters: a distance modulus of $m - M =$

24.47 (McConnachie et al. 2005), center coordinates $\alpha_{\text{J}2000} = 0^{\text{h}}42^{\text{m}}44\overset{\text{s}}{.}3$, $\delta_{\text{J}2000} = 41^{\circ}16'09''$ (NASA Extragalactic Database), a major axis position angle of 38° (de Vaucouleurs 1958), and a disk inclination angle to the line of sight of 75° (Gordon et al. 2006).

V -band magnitude and $B - V$ color histograms of the catalog objects are shown in Figure 2. Shaded histograms show a sub-sample of 77 objects identified in the *HST* frames.

Observed color-color diagrams of star cluster candidates, overplotted with simple stellar population (SSP) models of metallicity $Z = 0.008$ and ages ranging from 1 Myr to 15 Gyr, computed with PÉGASE (Fioc & Rocca-Volmerange 1997), are presented in Figure 3. Default PÉGASE parameters and a universal initial mass function (Kroupa 2002) were applied. Reddening vectors are depicted by applying the standard extinction law: a V -band extinction to color excess ratio $A_V/E(B-V) = 3.1$ and color excess ratios $E(U-B)/E(B-V) = 0.72$, $E(R-I)/E(B-V) = 0.69$. The Milky Way interstellar extinction in the direction of the M31 SW field is $E(B-V) = 0.062$ (Schlegel et al. 1998).

Figure 3, together with multiband color maps, suggests that the present sample covers a wide range of stellar populations, from old globular clusters through young massive clusters. Some objects, suspected to be young and heavily reddened in the $U - B$ vs. $B - V$ diagram, are displaced in opposite $R - I$ directions from the bulk of objects in the $R - I$ vs. $B - V$ diagram, making a large scatter. A detailed color analysis of these cases, taking into account multiband color maps, reveals two main reasons: $R - I$ is increased due to an additional flux from red background stars in the I -band, and $R - I$ is decreased by an additional contribution from the $H\alpha$ emission in the R band.

Combined multiband color maps (Figure Set 4.001-4.285; see Appendix B for description) of 285 objects are provided in the electronic edition of the *Supplement*. They serve as an illustrative material showing the objects' structure, the location of the aperture used for photometry, individual background conditions, and position in the survey field. These maps are also a valuable tool for revealing cluster interrelations with a global framework of various M31 galaxy components.

5. Summary

We have performed the Suprime-Cam survey of star clusters in the southwest field of the M31 disk up to $V \sim 20.5$ mag, providing the $UBVRI$ CCD aperture photometry catalog of 285 cluster candidates. The catalog includes 77 objects located in the *HST* frames. Photometry was performed through individually selected small apertures. Object cross-identifications with Galleti et al. (2007) and Krienke & Hodge (2007) are provided for

69 and 24 objects, respectively. Multiband color maps combined from LGGS (U , B , V , I , and $H\alpha$ bands), *GALEX* (NUV, FUV), 2MASS (J , H , and K_s bands), *Spitzer* (24 μm), and HI (21 cm) images, are available in the electronic edition of the *Supplement*.

This catalog contains an almost complete homogeneous sample of target objects in the surveyed area and will serve as a basis for follow-up imaging or spectroscopic studies. The presented materials suggest that the sample in the catalog covers a wide range of stellar population – from old globular clusters through young massive clusters. An analysis of the catalog will be forthcoming (Vansevičius et al. 2009).

We are indebted to Ieva Šablevičiūtė for her help with the BAOLAB/ISHAPE package. We are thankful to the anonymous referee for constructive suggestions. This work was financially supported in part by a Grant of the Lithuanian State Science and Studies Foundation. The star cluster survey is based on the Suprime-Cam images, collected at the Subaru Telescope, which is operated by the National Astronomical Observatory of Japan. The research is based in part on archival data obtained with the *Spitzer Space Telescope*, and has made use of the NASA/IPAC Extragalactic Database (NED) and the NASA/IPAC Infrared Science Archive, which are operated by the Jet Propulsion Laboratory, California Institute of Technology, under contract with the National Aeronautics and Space Administration; the SAOImage DS9, developed by Smithsonian Astrophysical Observatory; and the USNOFS Image and Catalogue Archive operated by the United States Naval Observatory, Flagstaff Station. The data presented in this paper were partly obtained from the Multimission Archive at the Space Telescope Science Institute.

A. *HST* Frames

The Multimission Archive at the Space Telescope Science Institute (MAST)³ was searched for *HST* frames overlapping with the Suprime-Cam survey field and publicly available to the date of 7 August 2007. Flat-fielded frames were cleaned of cosmic rays and corrected for distortions by employing procedures of the IRAF’s STSDAS package. The World Coordinate System information was corrected for all *HST* frames by referencing the Suprime-Cam V -band image, which was registered to the USNO-B1.0 catalog system. The numbers of analyzed *HST* data sets/telescope pointings overlapping with the studied Suprime-Cam field are: 222/29 (WFPC2), 9/3 (ACS), 43/6 (STIS), and 75/19 (NICMOS). Star cluster candidates from the catalog, presented in Table 2, have been identified only in the WFPC2 (71)

³*HST*: <http://archive.stsci.edu/hst/search.php>.

and the ACS (6) frames – 77 objects in total.

B. Multiband Color Maps

The LGGS mosaic images (Massey et al. 2006) in the U , B , V , I , and $H\alpha$ bands of the F7 or F8 fields were used for a multiband map construction. For objects located to the south of the F7 field, images of lower resolution from field F8 were substituted.

The 2MASS J , H , and K_s band “1 \times ” and “6 \times ” survey images were retrieved from the NASA/IPAC Infrared Science Archive⁴ and co-added to increase their signal-to-noise ratio. In general, the “6 \times ” co-added image was used, except for the gap region in the north of the surveyed field, where the “1 \times ” image was substituted. The *GALEX* NUV and FUV images by Gil de Paz et al. (2006) were retrieved from the *GALEX* Atlas of Nearby Galaxies⁵ and co-added to increase a signal-to-noise ratio. The *Spitzer* MIPS (24 μm) post-BCD (basic calibrated data) images of M31 (Program ID 99; PI: G. Rieke) were retrieved from the *Spitzer Space Telescope* Science Center Data Archive⁶, and mosaicked using the SWarp⁷ package (author E. Bertin).

The HI (21 cm) image was retrieved from the National Radio Astronomy Observatory image gallery⁸ (image courtesy of NRAO/AUI and David Thilker [JHU], Robert Braun [ASTRON], WSRT). It was converted from the TIFF to the FITS format using ImageTOOLSc⁹. The sky coordinate grid indicated by Westmeier et al. (2005) in their Figure 1 on the same HI image, was used for the initial registration. Fine adjustments were made assuming a global correlation between the *Spitzer* (24 μm) and HI (21 cm) source distributions, noted by Gordon et al. (2006).

The Suprime-Cam V -band mosaic image coordinate system was used as a reference to register and transform all images to the homogeneous pixel scale of 0.2 $''$ pixel $^{-1}$. The IRAF’s `geotran` procedure was used for the LGGS, *GALEX*, and 2MASS image transformations; the `wregister` procedure was used for the *Spitzer* (24 μm) and HI (21 cm) images. Most

⁴2MASS: <http://irsa.ipac.caltech.edu/>.

⁵*GALEX*: http://archive.stsci.edu/prepds/galex_atlas/index.html.

⁶*Spitzer*: <http://ssc.spitzer.caltech.edu/archanaly/>.

⁷See <http://terapix.iap.fr/>.

⁸HI: <http://www.nrao.edu/imagegallery/php/level3.php?id=475>.

⁹See <http://arnholm.org/software/index.htm>.

defects were masked prior to transformations. Since the LGGS images cover a wide wavelength range, they served as a reference for registering other images. A visual inspection was carried out to ensure an accurate coordinate match of the images prepared for a multiband map production. The FWHM and original pixel scale values of those images are provided in Table 1.

The sub-images of $80'' \times 80''$, centered on the objects' position, were cut out from the transformed images. SAOImage DS9 was employed to combine them into multiband color maps. The LGGS, 2MASS, and *GALEX* sub-images are displayed in a linear intensity scale, and the *Spitzer* sub-images are displayed in a square root scale. The minimal shown data level is individual for each sub-image, depending on the background intensity; however, the range of displayed intensities was kept constant for all objects. The constant displayed intensity limits across the surveyed area were applied only for HI (21 cm) sub-images and are overplotted with contour lines. A gray-shaded inset shows a global HI emission intensity, with black standing for the highest and white – for the lowest signal level over the survey area. Note, however, that the HI image is converted from the TIFF format and does not represent a real 21 cm emission distribution, serving for illustrative purposes only.

An example of the online multiband color maps and a layout template are shown in Figure 4. Since the displayed intensity range is kept constant for all objects, colors of individual objects are roughly preserved. However, the real emission level at $24\mu\text{m}$ should be estimated by referencing the object's position in the global *Spitzer* image of the survey field. Multiband maps for all 285 objects are provided in a Figure Set 4.001-4.285, published only in the electronic edition of the *Journal*.

REFERENCES

- Barmby, P., Holland, S., & Huchra, J. P. 2002, AJ, 123, 1937
Barmby, P., McLaughlin, D. E., Harris, W. E., Harris, G. L. H., & Forbes, D. A. 2007, AJ, 133, 2764
Cohen, J. G., Matthews, K., & Cameron, P. B. 2005, ApJ, 634, L45
Fioc, M., & Rocca-Volmerange, B. 1997, A&A, 326, 950
Galletti, S., Federici, L., Bellazzini, M., Fusi Pecci, F., & Macrina, S. 2004, A&A, 416, 917
Galletti, S., Bellazzini, M., Federici, L., Buzzoni, A., & Fusi Pecci, F. 2007, A&A, 471, 127
Gil de Paz, A., et al. 2007, ApJS, 173, 185

- Gordon, K. D., et al. 2006, ApJ, 638, L87
- Kim, S. C., et al. 2007, AJ, 134, 706
- Kodaira, K., Vansevičius, V., Bridžius, A., Komiyama, Y., Miyazaki, S., Stonkutė, R., Šablevičiūtė, I., & Narbutis, D. 2004, PASJ, 56, 1025 (Paper I)
- Krienke, O. K., & Hodge, P. W. 2007, PASP, 119, 7
- Kroupa, P. 2002, Science, 295, 82
- Larsen, S. S. 1999, A&AS, 139, 393
- Massey, P., Olsen, K. A. G., Hodge, P. W., Strong, S. B., Jacoby, G. H., Schlingman, W., & Smith, R. C. 2006, AJ, 131, 2478
- McConnachie, A. W., Irwin, M. J., Ferguson, A. M. N., Ibata, R. A., Lewis, G. F., & Tanvir, N. 2005, MNRAS, 356, 979
- Miyazaki, S., et al. 2002, PASJ, 54, 833
- Narbutis, D., Vansevičius, V., Kodaira, K., Šablevičiūtė, I., Stonkutė, R., & Bridžius, A. 2006, Baltic Astronomy, 15, 461
- Narbutis, D., Stonkutė, R., & Vansevičius, V. 2006, Baltic Astronomy, 15, 471
- Narbutis, D., Vansevičius, V., Kodaira, K., Bridžius, A., & Stonkutė, R. 2007, Baltic Astronomy, 16, 409
- Šablevičiūtė, I., Vansevičius, V., Kodaira, K., Narbutis, D., Stonkutė, R., & Bridžius, A. 2006, Baltic Astronomy, 15, 547
- Šablevičiūtė, I., Vansevičius, V., Kodaira, K., Narbutis, D., Stonkutė, R., & Bridžius, A. 2007, Baltic Astronomy, 16, 397
- Schlegel, D. J., Finkbeiner, D. P., & Davis, M. 1998, ApJ, 500, 525
- Stetson, P. B. 1987, PASP, 99, 191
- Tody, D. 1993, Astronomical Data Analysis Software and Systems II, 52, 173
- de Vaucouleurs, G. 1958, ApJ, 128, 465
- Westmeier, T., Braun, R., & Thilker, D. 2005, A&A, 436, 101

Table 1. Parameters of Original Images.

Source	Images	FWHM ["]	Scale ["/pixel ⁻¹]
Suprime-Cam	<i>B, V, R, Hα</i>	0.6–0.7	0.20
LGGS ^a	<i>U, B, V, R, I, Hα</i>	0.7–1.3	0.27
<i>GALEX</i> ^b	FUV, NUV	~4.5, ~5.5	1.50
2MASS	<i>J, H, K_s</i>	~3.5	1.00
<i>Spitzer</i>	24 μ m	~6.0	2.45
HI ^c	21 cm	...	10.3

^aMosaic images of the F6–F9 fields.

^bA strongly variable asymmetric PSF.

^cA TIFF format image.

Table 2. $UBVRI$ photometry data of the star cluster candidates in the M31 SW field.

ID ^a	α_{J2000}	δ_{J2000}	V^b	$U-B$	$B-V$	$V-R$	$R-I$	σ_V	σ_{U-B}	σ_{B-V}	σ_{V-R}	σ_{R-I}	n^c Ap ^d	HST^e	CrossID ^f	
KW001	10.042834	40.607317	18.791	-0.259	0.295	0.306	0.450	0.012	0.022	0.022	0.016	0.025	3	3.2	W	1: BH02
KW002	10.044094	40.580988	19.963	0.197	0.636	0.473	0.524	0.016	0.027	0.025	0.022	0.028	3	3.0	W	...
KW003	10.045193	40.897594	19.575	-0.256	0.211	0.241	0.353	0.013	0.035	0.022	0.018	0.022	2	3.0
KW004	10.045684	40.603264	18.497	-0.419	0.203	0.222	0.268	0.013	0.031	0.017	0.017	0.017	3	3.0	W	2:37, 3: C01
KW005	10.049319	40.585042	19.467	-0.599	0.945	0.690	0.750	0.019	0.025	0.025	0.023	0.020	3	3.0	W	...
KW006	10.054298	40.605353	18.711	-0.231	0.283	0.284	0.429	0.013	0.023	0.021	0.021	0.026	3	3.4	W	...
KW007	10.054684	40.691637	20.513	0.124	0.618	0.510	0.651	0.028	0.031	0.037	0.037	0.047	2	3.0
KW008	10.056707	40.638101	19.640	-0.282	0.379	0.354	0.426	0.016	0.020	0.022	0.022	0.032	3	3.0	W	...
KW009	10.057000	40.767726	20.620	-0.362	0.331	0.837	1.527	0.030	0.029	0.038	0.037	0.026	2	3.0	W	...
KW010	10.057682	40.675488	20.114	0.285	0.801	0.593	0.837	0.019	0.037	0.031	0.030	0.030	2	3.6
KW011	10.059244	40.655842	18.783	-0.263	0.255	0.226	0.332	0.025	0.020	0.030	0.030	0.023	3	3.6	...	3: C02
KW012	10.059651	40.604218	19.863	0.084	0.287	0.219	0.240	0.016	0.033	0.034	0.026	0.032	3	3.0	W	2:44
KW013	10.060667	40.622445	18.562	-0.399	0.041	0.095	0.122	0.011	0.017	0.016	0.016	0.017	3	3.0	W	3: C03
KW014	10.061770	40.772343	20.357	-0.208	0.531	0.467	0.694	0.020	0.028	0.030	0.031	0.041	2	3.4
KW015	10.062032	40.757713	20.441	0.262	0.583	0.366	0.345	0.018	0.030	0.027	0.030	0.048	2	3.0	W	...
KW016	10.064046	40.615179	18.571	-0.215	0.308	0.262	0.405	0.025	0.039	0.030	0.027	0.017	3	3.2	W	1: SK043B, 3: C04
KW017	10.064532	40.666578	18.484	-0.269	0.303	0.286	0.387	0.011	0.016	0.016	0.016	0.016	3	3.4	...	1: B189D, 3: C05
KW018	10.064682	40.773154	19.800	0.074	0.603	0.469	0.535	0.016	0.027	0.025	0.025	0.026	2	3.0	...	1: SK078C
KW019	10.065037	40.588203	20.126	0.112	0.365	0.279	0.434	0.016	0.031	0.029	0.024	0.042	3	3.0	W	...
KW020	10.065188	40.598566	20.333	0.178	0.693	0.464	0.513	0.019	0.040	0.036	0.027	0.036	3	3.4	W	...
KW021	10.066683	40.760506	20.316	-0.916	-0.032	0.056	-0.146	0.021	0.024	0.029	0.038	0.082	2	3.0
KW022	10.071942	40.651375	18.121	-0.431	0.119	0.159	0.235	0.011	0.020	0.021	0.016	0.022	3	3.6	...	1: B322, 3: C06
KW023	10.072371	40.791581	19.538	-0.113	0.449	0.447	0.841	0.015	0.025	0.024	0.022	0.023	2	3.6
KW024	10.072486	40.546082	20.335	-0.333	0.246	0.262	0.486	0.030	0.029	0.036	0.037	0.038	3	3.0
KW025	10.072892	40.580773	19.894	0.420	1.053	0.684	0.842	0.019	0.053	0.035	0.025	0.028	3	4.0	W	...
KW026	10.073128	40.655588	18.558	-0.290	0.078	0.117	0.171	0.012	0.021	0.021	0.017	0.019	3	3.0	...	3: C07
KW027	10.073624	40.552309	19.865	-0.149	0.328	0.314	0.479	0.017	0.026	0.027	0.024	0.034	3	3.0
KW028	10.076114	40.545728	18.562	0.114	0.413	0.293	0.386	0.013	0.017	0.018	0.018	0.021	3	3.6	...	1: B323, 3: C08
KW029	10.076494	40.661792	19.977	-0.409	-0.025	0.053	0.114	0.018	0.023	0.024	0.029	0.047	3	3.0
KW030	10.078454	40.520986	19.320	0.279	1.570	0.768	0.854	0.015	0.048	0.027	0.022	0.031	2	3.0	...	1: SK044B, 3: C09
KW031	10.078486	40.668040	18.491	-0.516	0.079	0.155	0.277	0.011	0.019	0.016	0.016	0.020	3	3.4
KW032	10.079443	40.635403	19.525	-0.172	0.438	0.405	0.575	0.013	0.021	0.021	0.019	0.021	3	3.0
KW033	10.080917	40.624806	18.688	-0.195	0.383	0.336	0.470	0.012	0.019	0.018	0.017	0.017	3	3.0	...	1: B442, 3: C10
KW034	10.081736	40.589773	20.542	-0.137	0.342	0.352	0.568	0.028	0.033	0.036	0.039	0.047	3	3.0	W	...
KW035	10.081742	40.711390	19.522	-0.206	0.265	0.257	0.371	0.014	0.022	0.020	0.026	0.032	2	3.0
KW036	10.082864	40.591933	19.476	-0.426	0.523	0.551	0.791	0.017	0.031	0.028	0.021	0.020	3	3.0	W	...
KW037	10.082959	40.513220	18.735	-0.180	0.160	0.140	0.171	0.012	0.020	0.020	0.020	0.021	2	3.4	...	3: C11
KW038	10.083860	40.509409	19.816	0.153	0.455	0.355	0.435	0.014	0.030	0.029	0.021	0.023	2	3.0
KW039	10.084620	40.732913	15.688	0.366	0.984	0.597	99.999	0.010	0.018	0.014	0.018	99.999	2	7.0	...	1: B005
KW040	10.086591	40.556094	18.933	-0.210	0.254	0.238	0.329	0.017	0.017	0.021	0.021	0.018	3	3.0	...	1: B443
KW041	10.087815	40.627581	20.416	-0.303	0.138	0.102	0.232	0.022	0.029	0.033	0.031	0.044	3	3.0
KW042	10.089288	40.620743	19.610	0.160	0.491	0.342	0.498	0.014	0.025	0.025	0.020	0.023	3	3.2
KW043	10.093248	40.637963	19.522	-0.329	0.379	0.395	0.550	0.014	0.020	0.021	0.020	0.020	3	3.0
KW044	10.096228	40.513202	17.471	0.003	0.681	0.463	0.543	0.016	0.016	0.019	0.019	0.015	2	6.8	...	1: B325, 3: C12
KW045	10.096736	40.621046	19.783	0.089	0.342	0.319	0.542	0.016	0.022	0.022	0.022	0.023	3	3.0
KW046	10.097930	40.649232	19.162	-0.410	0.243	0.228	0.408	0.014	0.023	0.020	0.020	0.022	3	3.2

Table 2—Continued

ID ^a	$\alpha_{\text{J}2000}$	$\delta_{\text{J}2000}$	V^{b}	$U-B$	$B-V$	$V-R$	$R-I$	σ_V	σ_{U-B}	σ_{B-V}	σ_{V-R}	σ_{R-I}	$n^{\text{c}} \text{Ap}^{\text{d}} HST^{\text{e}}$	CrossID ^f
KW047	10.098491	40.520264	19.921	-0.157	0.304	0.297	0.450	0.019	0.027	0.028	0.026	0.029	2 3.0	...
KW048	10.100420	40.606290	16.876	-0.491	0.212	0.281	0.448	0.010	0.022	0.014	0.014	0.015	3 4.4	...
KW049	10.100878	40.533352	19.198	-0.326	0.124	0.158	0.157	0.013	0.030	0.029	0.020	0.024	3 3.0	...
KW050	10.101098	40.685456	19.818	-0.351	-0.004	0.057	0.062	0.017	0.023	0.025	0.030	0.045	2 3.0	...
KW051	10.101208	40.617240	20.514	-0.049	0.127	0.122	-0.032	0.028	0.028	0.035	0.046	0.080	3 3.0	...
KW052	10.101897	40.905033	20.000	-0.484	0.551	0.345	0.375	0.023	0.032	0.033	0.033	0.035	2 3.2	...
KW053	10.103406	40.812996	19.224	0.167	0.556	0.426	0.583	0.013	0.023	0.020	0.022	0.022	2 3.0	... 1:SK014A, 3:C14
KW054	10.103628	40.816919	19.689	0.227	0.794	0.580	0.661	0.018	0.033	0.030	0.027	0.026	2 3.0	... 3:C15
KW055	10.104183	40.554877	19.615	-0.340	0.116	0.118	0.170	0.016	0.023	0.023	0.028	0.035	3 3.0	...
KW056	10.105344	40.813521	19.331	0.158	0.589	0.420	0.587	0.014	0.021	0.021	0.020	0.022	2 3.6	...
KW057	10.108014	40.628148	19.320	0.169	1.160	0.777	0.834	0.013	0.032	0.029	0.017	0.020	3 3.0	... 3:C16
KW058	10.109058	40.758864	20.155	-0.057	0.505	0.474	0.798	0.021	0.029	0.029	0.030	0.029	2 3.0	W 1:SK015A
KW059	10.110855	40.792590	19.254	0.134	0.550	0.436	0.689	0.013	0.022	0.022	0.021	0.021	2 3.0	...
KW060	10.111907	40.948786	19.837	-0.182	0.011	0.023	-0.024	0.022	0.030	0.031	0.034	0.045	1 3.0	...
KW061	10.112229	40.532622	19.951	0.177	0.728	0.554	0.804	0.019	0.039	0.032	0.025	0.025	3 3.0	...
KW062	10.113666	40.756774	18.727	-0.218	0.215	0.239	0.347	0.012	0.020	0.020	0.020	0.021	2 3.0	W 2:46, 3:C17
KW063	10.114264	40.734285	18.523	-1.080	-0.167	0.021	0.032	0.012	0.019	0.020	0.021	0.031	2 3.0	W 3:E09
KW064	10.114489	40.667752	19.901	-0.239	0.319	0.282	0.440	0.020	0.022	0.026	0.027	0.031	3 3.0	...
KW065	10.114689	40.511684	20.458	-0.005	0.311	0.251	0.116	0.024	0.048	0.044	0.036	0.049	2 3.0	...
KW066	10.115251	40.528377	19.549	-0.475	0.067	0.138	0.253	0.014	0.038	0.037	0.022	0.031	3 3.0	...
KW067	10.115544	40.772098	20.276	-0.190	1.152	0.792	0.942	0.021	0.079	0.076	0.031	0.029	2 3.0	W ...
KW068	10.117164	40.544111	20.416	0.186	0.417	0.273	0.359	0.028	0.037	0.037	0.035	0.036	3 3.0	...
KW069	10.118468	40.770439	20.088	-0.074	0.623	0.488	0.609	0.019	0.032	0.031	0.029	0.031	2 3.0	W ...
KW070	10.121350	40.858484	20.322	0.716	1.200	0.759	0.856	0.023	0.052	0.039	0.033	0.033	2 3.0	...
KW071	10.121597	40.624824	20.409	-0.322	0.249	0.221	0.335	0.029	0.039	0.038	0.045	0.062	3 3.0	...
KW072	10.122547	40.604198	15.288	-0.522	0.191	0.232	0.355	0.013	0.020	0.016	0.016	0.022	3 7.0	... 1:VDB0
KW073	10.122585	40.779680	20.393	-0.474	0.071	0.130	0.353	0.031	0.032	0.041	0.053	0.078	2 3.0	W ...
KW074	10.123130	40.689759	20.147	-0.068	0.623	0.510	0.796	0.017	0.039	0.026	0.027	0.030	2 3.0
KW075	10.123280	40.545685	20.124	0.101	0.524	0.353	0.456	0.020	0.031	0.029	0.029	0.036	3 3.0	...
KW076	10.123870	40.638422	20.309	0.236	0.538	0.393	0.527	0.022	0.033	0.030	0.030	0.033	3 3.0	...
KW077	10.124485	40.515316	20.516	0.240	0.505	0.381	0.505	0.024	0.056	0.037	0.038	0.042	2 3.0	...
KW078	10.127077	40.758183	16.387	-0.696	0.003	0.120	0.254	0.010	0.018	0.014	0.014	0.023	2 3.0	W 1:BH05
KW079	10.127645	40.748311	17.835	-0.846	-0.055	0.119	0.483	0.012	0.020	0.017	0.021	0.024	2 3.0	W 1:BH06
KW080	10.128343	40.708480	19.666	-1.154	0.146	0.628	-0.604	0.019	0.030	0.030	0.028	0.048	2 3.0	W 3:E11
KW081	10.128610	40.836477	20.220	0.272	0.673	0.523	0.651	0.023	0.031	0.031	0.030	0.032	2 3.0	...
KW082	10.128724	40.784160	19.422	-0.252	0.224	0.198	0.270	0.013	0.032	0.029	0.020	0.025	2 3.0	W ...
KW083	10.128995	40.712495	18.858	-1.047	-0.147	-0.066	-0.078	0.013	0.020	0.018	0.025	0.035	2 3.0	W ...
KW084	10.130689	40.752391	19.818	-0.905	-0.047	0.198	0.649	0.031	0.043	0.045	0.044	0.044	2 3.0	W 2:50
KW085	10.132159	40.517604	20.587	-0.034	0.327	0.437	0.948	0.022	0.035	0.035	0.034	0.032	2 3.0	...
KW086	10.133395	40.744845	19.180	-0.650	0.011	0.053	0.027	0.019	0.026	0.027	0.028	0.035	2 3.0	W 2:51
KW087	10.134043	40.774174	20.437	0.222	0.831	0.528	0.667	0.024	0.046	0.038	0.037	0.044	2 3.0	W ...
KW088	10.135427	40.857746	20.646	-1.006	0.007	0.505	-1.037	0.023	0.025	0.030	0.034	0.118	2 3.0	... 3:E16
KW089	10.135717	40.837140	19.140	-0.128	0.258	0.230	0.284	0.012	0.020	0.017	0.021	0.023	2 3.0	... 3:C18
KW090	10.135866	40.624524	19.979	-0.449	0.193	0.178	0.247	0.020	0.039	0.025	0.027	0.032	3 3.0	...
KW091	10.139704	40.721005	18.688	-0.917	-0.112	-0.004	0.037	0.015	0.022	0.021	0.023	0.031	2 3.0	W 2:53
KW092	10.140931	40.546191	19.461	-0.579	0.824	0.167	-0.522	0.016	0.028	0.027	0.026	0.047	3 3.6	... 3:E18

Table 2—Continued

ID ^a	$\alpha_{\text{J}2000}$	$\delta_{\text{J}2000}$	V^{b}	$U-B$	$B-V$	$V-R$	$R-I$	σ_V	σ_{U-B}	σ_{B-V}	σ_{V-R}	σ_{R-I}	$n^{\text{c}} \text{Ap}^{\text{d}} HST^{\text{e}}$	CrossID ^f	
KW093	10.142016	40.721744	17.036	-0.641	0.556	0.407	0.442	0.011	0.021	0.016	0.015	0.023	2 3.0	W	...
KW094	10.143789	40.808330	20.148	-0.147	0.645	0.658	0.897	0.023	0.043	0.044	0.032	0.030	2 3.0
KW095	10.144465	40.594830	19.332	-0.774	0.464	0.562	0.067	0.016	0.026	0.022	0.022	0.027	3 3.0	...	3:E19
KW096	10.148474	40.930105	20.596	-0.067	0.839	0.670	0.781	0.033	0.044	0.046	0.044	0.042	1 3.0
KW097	10.149876	40.651920	19.560	-0.109	0.588	0.400	0.527	0.034	0.020	0.037	0.036	0.021	3 3.0	...	1:SK051B
KW098	10.150477	40.621818	20.461	-0.783	0.041	0.089	0.115	0.022	0.024	0.029	0.036	0.052	3 3.0
KW099	10.151301	40.849434	19.733	0.236	0.774	0.526	0.566	0.015	0.026	0.025	0.023	0.023	2 3.0
KW100	10.152200	40.670904	19.026	0.029	0.636	0.460	0.568	0.016	0.019	0.021	0.020	0.017	3 3.0	...	1:B448, 3:C19
KW101	10.154751	40.556076	20.194	0.327	0.736	0.516	0.643	0.026	0.060	0.044	0.034	0.032	3 3.0	W	1:BH09
KW102	10.155186	40.654073	19.152	-0.076	0.671	0.456	0.585	0.019	0.019	0.023	0.022	0.019	3 3.4	...	3:C20
KW103	10.155619	40.812697	19.253	-0.152	0.300	0.239	0.288	0.013	0.021	0.022	0.022	0.027	2 3.0	...	1:B006D, 3:C21
KW104	10.155877	40.923688	19.642	0.912	1.611	1.057	1.255	0.024	0.052	0.038	0.032	0.030	1 3.0
KW105	10.158370	40.774675	20.487	-0.253	0.195	0.136	0.101	0.027	0.030	0.034	0.044	0.075	2 3.0	W	...
KW106	10.160499	40.748158	20.337	0.339	0.758	0.516	0.602	0.021	0.037	0.034	0.030	0.030	2 3.0
KW107	10.161471	40.528937	20.553	0.153	0.401	0.213	-0.060	0.022	0.032	0.032	0.043	0.080	3 3.0
KW108	10.163799	40.625910	20.089	-0.981	0.385	0.782	-0.331	0.020	0.029	0.033	0.024	0.029	3 3.2	...	3:E25
KW109	10.163812	40.581285	18.497	-0.156	0.631	0.427	0.493	0.011	0.019	0.017	0.016	0.016	3 3.0	W	...
KW110	10.164209	40.802038	20.169	0.179	0.608	0.345	0.180	0.019	0.041	0.039	0.031	0.055	2 3.4
KW111	10.172061	40.819370	20.224	-0.643	0.007	0.075	-0.014	0.020	0.023	0.025	0.033	0.057	2 3.0
KW112	10.173634	40.641151	18.726	0.509	1.218	0.753	0.889	0.013	0.025	0.019	0.017	0.016	3 3.4	...	1:B335, 3:C22
KW113	10.176121	40.601310	19.227	0.204	0.757	0.472	0.551	0.012	0.019	0.018	0.017	0.023	3 3.0	...	1:B449, 3:C23
KW114	10.176708	40.760944	19.928	0.560	1.262	0.821	1.087	0.018	0.049	0.040	0.025	0.023	2 3.0
KW115	10.178076	40.839455	20.103	-0.233	0.176	0.191	0.310	0.016	0.023	0.025	0.028	0.038	2 3.0
KW116	10.179689	40.830911	20.544	-0.899	0.004	0.164	0.194	0.028	0.025	0.035	0.041	0.057	2 3.0
KW117	10.182641	40.958843	20.265	-0.675	0.233	0.295	0.251	0.027	0.033	0.037	0.041	0.048	1 3.0
KW118	10.184256	40.754105	20.108	-1.064	-0.034	0.405	-0.793	0.016	0.030	0.025	0.028	0.076	2 3.0	...	3:E30
KW119	10.184457	40.5677926	19.583	-0.231	0.511	0.410	0.598	0.014	0.020	0.021	0.020	0.021	3 3.0
KW120	10.185198	40.620481	19.679	0.444	1.167	0.755	0.923	0.013	0.028	0.022	0.018	0.017	3 3.0
KW121	10.186508	40.508358	19.959	0.166	0.750	0.527	99.999	0.014	0.027	0.023	0.026	99.999	2 3.2
KW122	10.187020	40.885639	19.810	0.283	0.652	0.444	0.666	0.016	0.036	0.034	0.023	0.052	2 3.0	W	1:BH10
KW123	10.192081	40.959220	19.902	-0.062	0.187	0.168	0.160	0.022	0.031	0.032	0.032	0.035	1 3.0
KW124	10.193355	40.861358	19.178	-0.191	0.389	0.319	0.435	0.013	0.021	0.022	0.020	0.023	2 3.2	...	3:C25
KW125	10.195821	40.682801	19.361	0.211	0.790	0.477	0.536	0.013	0.024	0.020	0.022	0.026	2 3.6	W	1:DAO38
KW126	10.198084	40.668783	20.351	-0.136	1.414	0.687	0.893	0.022	0.048	0.044	0.038	0.038	3 4.0
KW127	10.198833	40.632812	20.110	0.420	0.870	0.557	0.653	0.022	0.041	0.029	0.027	0.022	3 3.0
KW128	10.199074	40.985069	18.459	-1.351	0.401	0.291	-0.499	0.012	0.024	0.019	0.017	0.022	2 4.0	...	1:V203, 3:E33
KW129	10.199189	40.926257	19.706	-0.045	0.261	0.230	0.287	0.021	0.039	0.036	0.031	0.033	2 3.0	...	1:V202
KW130	10.200178	40.517261	19.787	0.194	0.716	0.453	0.528	0.014	0.025	0.024	0.021	0.026	2 3.0
KW131	10.200306	40.677835	20.196	0.378	0.958	0.617	0.902	0.020	0.040	0.034	0.028	0.029	2 4.0	...	1:SK088C
KW132	10.201478	40.866229	18.619	-0.435	0.262	0.317	0.493	0.015	0.032	0.019	0.019	0.020	3 3.0	...	3:C27
KW133	10.201479	40.585044	18.412	-0.113	0.294	0.250	0.387	0.011	0.016	0.016	0.016	0.017	3 3.0	...	1:B452, 3:C26
KW134	10.202329	40.960126	19.282	0.259	0.548	0.390	0.573	0.013	0.022	0.019	0.019	0.022	2 3.0	...	3:C28
KW135	10.203616	40.565628	19.646	-0.229	0.269	0.283	0.433	0.017	0.025	0.026	0.025	0.027	3 3.0
KW136	10.204916	40.648672	19.671	0.064	0.455	0.312	0.406	0.014	0.020	0.021	0.021	0.031	3 3.0
KW137	10.205833	40.692273	18.282	0.260	0.804	0.502	0.622	0.011	0.020	0.019	0.015	0.019	2 3.4	W	1:B018, 3:C29
KW138	10.206908	40.890597	20.041	-0.351	0.051	0.094	0.312	0.021	0.022	0.027	0.032	0.059	3 3.0

Table 2—Continued

ID ^a	$\alpha_{\text{J}2000}$	$\delta_{\text{J}2000}$	V^{b}	$U-B$	$B-V$	$V-R$	$R-I$	σ_V	σ_{U-B}	σ_{B-V}	σ_{V-R}	σ_{R-I}	n^{c}	Ap ^d	HST ^e	CrossID ^f
KW139	10.211783	40.677370	20.463	0.536	1.044	0.643	0.798	0.021	0.064	0.032	0.032	0.036	2	3.0	W	1:BH11
KW140	10.214572	40.557683	19.300	0.169	0.655	0.447	0.687	0.015	0.026	0.021	0.020	0.025	3	3.2	...	1:B198D, 3:C30
KW141	10.215041	40.735078	17.985	-0.448	0.740	0.669	1.114	0.011	0.019	0.019	0.015	0.019	2	4.2	W	1:B011D, 3:C31
KW142	10.217001	40.583774	19.985	-0.139	0.403	0.334	0.494	0.018	0.027	0.029	0.030	0.034	3	3.0	W	...
KW143	10.217610	40.534843	20.585	0.042	0.366	0.236	0.358	0.021	0.046	0.030	0.041	0.047	3	3.0
KW144	10.217733	40.978228	19.444	0.236	0.623	0.449	0.568	0.013	0.035	0.022	0.018	0.019	2	3.0	...	1:B012D, 3:C33
KW145	10.217768	40.898999	19.287	0.407	0.937	0.568	0.662	0.012	0.025	0.019	0.017	0.018	3	3.2	...	1:B246, 3:C32
KW146	10.220359	40.868819	20.292	0.349	0.847	0.552	0.686	0.017	0.030	0.027	0.026	0.030	3	3.0
KW147	10.220614	40.588774	18.883	0.278	0.875	0.580	0.690	0.013	0.025	0.021	0.021	0.020	3	4.4	W	2:74, 3:C34
KW148	10.220852	40.538287	19.640	-0.883	0.217	0.568	0.095	0.014	0.019	0.020	0.020	0.020	3	3.0	...	3:E35
KW149	10.221971	40.732549	20.285	-0.346	0.570	0.307	0.232	0.021	0.035	0.034	0.033	0.058	2	3.0	W	2:75
KW150	10.222354	40.827422	20.577	0.434	1.391	0.752	0.865	0.019	0.047	0.038	0.026	0.028	3	3.0
KW151	10.223014	40.718869	20.596	0.331	0.643	0.529	0.682	0.020	0.035	0.029	0.028	0.032	2	3.0	W	2:76
KW152	10.223746	40.614171	20.354	0.246	0.928	0.595	0.655	0.038	0.038	0.045	0.042	0.029	3	3.0	W	2:77
KW153	10.224476	40.671365	20.480	0.191	0.447	0.239	0.154	0.021	0.030	0.031	0.038	0.069	3	3.0	W	2:78
KW154	10.228397	40.592104	19.799	-0.010	0.429	0.327	0.378	0.020	0.025	0.026	0.027	0.035	3	3.0	W	2:79, 2:80
KW155	10.228465	40.738911	20.106	0.205	0.744	0.465	0.562	0.017	0.027	0.025	0.025	0.031	2	3.0
KW156	10.230713	40.622441	20.550	0.026	0.573	0.435	0.697	0.019	0.028	0.028	0.029	0.032	3	3.0
KW157	10.232157	40.589603	20.103	-0.408	0.135	0.220	0.438	0.018	0.037	0.025	0.028	0.038	3	3.0	W	2:81
KW158	10.233583	40.706303	20.060	0.241	0.769	0.532	0.778	0.016	0.029	0.025	0.023	0.026	2	3.0	W	...
KW159	10.234748	40.578257	20.204	-0.017	0.397	0.293	0.493	0.019	0.027	0.027	0.030	0.042	3	3.0	W	2:83
KW160	10.236023	40.573705	19.473	-0.093	0.312	0.257	0.310	0.013	0.019	0.020	0.020	0.023	3	3.0	W	2:85
KW161	10.237263	40.609178	20.533	0.490	1.062	0.663	0.942	0.021	0.063	0.039	0.028	0.027	3	3.0	W	2:87
KW162	10.238067	40.587143	20.372	-0.326	0.261	0.240	0.224	0.021	0.029	0.031	0.035	0.057	3	3.0	W	2:88
KW163	10.238529	40.602163	19.722	-1.147	0.443	0.837	-0.145	0.016	0.025	0.024	0.021	0.028	3	3.0	W	3:E37
KW164	10.239532	40.740927	19.079	0.388	1.273	0.812	0.857	0.012	0.022	0.019	0.020	0.020	2	3.0	...	3:C35
KW165	10.239760	40.548735	19.803	-0.290	0.308	0.315	0.483	0.018	0.022	0.024	0.025	0.028	3	3.0
KW166	10.240497	40.572721	19.767	-0.451	0.025	0.090	0.272	0.015	0.025	0.021	0.026	0.035	3	3.0	W	2:93
KW167	10.242480	40.822994	19.969	0.061	0.364	0.320	0.338	0.016	0.021	0.023	0.024	0.036	3	3.0
KW168	10.243214	40.890785	20.425	0.019	1.421	0.728	0.982	0.020	0.056	0.040	0.029	0.030	3	3.0
KW169	10.243519	40.609815	19.084	-0.261	0.425	0.390	0.624	0.015	0.019	0.020	0.020	0.019	3	3.0
KW170	10.245036	40.573454	19.583	-0.144	0.317	0.337	0.506	0.014	0.021	0.021	0.020	0.021	3	3.0	W	2:97
KW171	10.245314	40.596664	14.259	0.122	0.808	0.505	99.999	0.010	0.014	0.014	0.022	99.999	3	10.0	W	1:B338
KW172	10.245397	40.718050	20.188	0.889	1.558	0.922	1.022	0.019	0.066	0.053	0.024	0.022	2	4.0	W	...
KW173	10.246629	40.584500	19.838	-0.182	0.345	0.302	0.361	0.016	0.032	0.024	0.024	0.037	3	3.0	W	2:100
KW174	10.247275	40.565062	20.288	0.058	0.339	0.288	0.491	0.022	0.031	0.031	0.035	0.041	3	3.0
KW175	10.249220	40.608032	19.908	-0.946	0.064	0.122	-0.082	0.016	0.024	0.024	0.029	0.050	3	3.0
KW176	10.251109	40.574466	19.989	-0.042	0.901	0.598	0.786	0.016	0.035	0.025	0.022	0.021	3	3.0	W	...
KW177	10.260625	40.840829	20.408	-0.090	0.309	0.312	0.428	0.021	0.025	0.029	0.038	0.051	3	3.0
KW178	10.260707	40.804317	19.365	0.498	1.672	0.794	0.846	0.013	0.038	0.026	0.019	0.023	3	3.6	...	1:SK092C
KW179	10.260999	40.578872	19.587	-0.139	0.171	0.185	0.386	0.017	0.039	0.024	0.026	0.029	3	3.0	W	2:113
KW180	10.261423	40.564231	19.404	-0.182	0.250	0.257	0.354	0.013	0.019	0.019	0.020	0.023	3	3.2
KW181	10.261856	40.696440	20.364	0.237	0.720	0.460	0.647	0.019	0.027	0.027	0.028	0.033	2	3.0
KW182	10.262026	40.582932	18.804	-0.223	0.240	0.239	0.344	0.012	0.017	0.017	0.023	0.023	3	3.0	W	1:BH12
KW183	10.262293	40.943278	20.384	0.559	1.164	0.653	0.697	0.021	0.053	0.034	0.030	0.036	2	3.0
KW184	10.265131	40.929020	20.307	0.349	0.885	0.553	0.719	0.021	0.034	0.031	0.029	0.032	2	3.0

Table 2—Continued

ID ^a	$\alpha_{\text{J}2000}$	$\delta_{\text{J}2000}$	V^{b}	$U-B$	$B-V$	$V-R$	$R-I$	σ_V	σ_{U-B}	σ_{B-V}	σ_{V-R}	σ_{R-I}	$n^{\text{c}} \text{ Ap}^{\text{d}} HST^{\text{e}}$	CrossID ^f
KW185	10.266634	40.539275	20.004	0.177	0.564	0.482	1.011	0.021	0.026	0.027	0.027	0.024	3 3.6	...
KW186	10.268358	40.664087	20.215	0.238	0.568	0.366	0.495	0.016	0.026	0.023	0.025	0.035	3 3.0	...
KW187	10.268969	40.578992	19.243	-0.501	0.234	0.305	0.475	0.013	0.018	0.019	0.018	0.019	3 3.0	...
KW188	10.271079	40.757788	20.259	0.140	0.644	0.427	0.545	0.026	0.031	0.034	0.037	0.040	2 3.0	...
KW189	10.272325	40.858677	19.936	-0.169	0.247	0.201	0.360	0.016	0.030	0.022	0.024	0.033	3 3.0	...
KW190	10.272486	40.583171	18.745	-0.375	0.229	0.289	0.501	0.013	0.017	0.017	0.017	0.016	3 3.0	...
KW191	10.274384	40.899863	19.984	0.125	0.502	0.405	0.453	0.020	0.028	0.027	0.029	0.037	3 3.4	...
KW192	10.275912	40.615670	20.309	-0.167	0.465	0.341	0.474	0.022	0.031	0.034	0.031	0.037	3 3.0	...
KW193	10.276009	40.603827	20.227	0.025	0.229	0.178	0.241	0.025	0.047	0.033	0.037	0.047	3 3.0	...
KW194	10.278571	40.574739	19.146	-0.223	0.313	0.286	0.379	0.012	0.026	0.018	0.018	0.026	3 3.0	...
KW195	10.280424	40.906253	20.343	0.192	0.587	0.335	0.156	0.021	0.030	0.031	0.035	0.056	3 3.6	...
KW196	10.283061	40.883640	18.698	0.237	0.947	0.585	0.613	0.015	0.019	0.020	0.019	0.021	3 3.0	...
KW197	10.283193	40.812401	20.385	-0.037	0.543	0.398	0.540	0.021	0.028	0.029	0.030	0.034	3 3.0	...
KW198	10.284429	40.547855	19.056	0.159	0.611	0.492	0.672	0.012	0.018	0.018	0.017	0.016	3 4.0	...
KW199	10.288141	40.598100	16.567	0.270	0.898	0.562	0.615	0.011	0.024	0.015	0.015	0.014	3 5.2	...
KW200	10.291607	40.969815	19.010	0.251	0.725	0.459	0.585	0.012	0.019	0.018	0.017	0.025	2 3.0	...
KW201	10.291765	40.533081	20.573	0.072	0.279	0.206	0.315	0.019	0.027	0.029	0.032	0.039	3 3.0	...
KW202	10.296751	40.6977354	20.480	-0.186	0.178	0.142	0.267	0.023	0.026	0.031	0.043	0.060	2 3.0	...
KW203	10.297747	40.805569	19.058	-0.393	0.271	0.344	0.635	0.013	0.031	0.018	0.018	0.018	3 3.0	...
KW204	10.298723	40.588541	20.321	-0.065	0.359	0.262	0.398	0.021	0.032	0.032	0.034	0.052	2 3.0	...
KW205	10.299204	40.738821	20.569	0.252	0.768	0.462	0.378	0.025	0.036	0.037	0.036	0.064	2 3.0	...
KW206	10.299839	40.963784	20.412	0.262	0.776	0.510	0.821	0.020	0.041	0.029	0.029	0.033	2 3.0	...
KW207	10.302041	40.673833	20.195	0.224	0.786	0.542	0.800	0.019	0.031	0.030	0.028	0.027	2 3.0	...
KW208	10.303265	40.571554	18.102	-0.165	0.255	0.267	0.520	0.011	0.019	0.019	0.019	0.022	2 3.6	...
KW209	10.304612	40.647583	20.563	0.217	0.465	0.287	0.390	0.018	0.030	0.027	0.029	0.050	2 3.0	A
KW210	10.307544	40.566140	18.313	-0.159	0.230	0.214	0.308	0.011	0.016	0.016	0.019	0.025	2 3.6	...
KW211	10.310518	40.930886	15.695	0.155	0.839	0.538	99.999	0.010	0.019	0.018	0.018	99.999	2 8.0	W
KW212	10.314922	40.818686	19.906	-0.388	0.042	0.033	-0.049	0.016	0.022	0.022	0.027	0.046	3 3.0	...
KW213	10.317812	40.868973	20.281	0.054	0.417	0.288	0.353	0.017	0.025	0.026	0.027	0.041	3 3.0	...
KW214	10.318702	40.984344	16.971	0.101	0.778	0.516	0.593	0.010	0.029	0.018	0.018	0.022	2 6.4	...
KW215	10.318876	40.650869	19.069	-0.329	0.258	0.181	0.320	0.012	0.017	0.017	0.017	0.029	2 3.0	A
KW216	10.319850	40.807304	20.562	0.110	0.294	0.194	-0.082	0.027	0.027	0.033	0.043	0.084	3 3.0	...
KW217	10.323727	40.729072	20.248	0.181	0.518	0.399	0.552	0.021	0.026	0.028	0.030	0.037	2 3.0	...
KW218	10.324434	40.726544	20.487	-0.562	1.003	0.660	0.615	0.022	0.049	0.037	0.032	0.035	2 3.0	...
KW219	10.325588	40.733722	19.187	0.226	0.542	0.362	0.515	0.012	0.021	0.021	0.018	0.022	2 3.2	...
KW220	10.326650	40.650434	19.156	-0.364	0.531	0.483	0.716	0.013	0.022	0.020	0.022	0.027	2 3.0	A
KW221	10.328017	40.954437	17.676	0.847	1.438	0.831	0.911	0.010	0.021	0.019	0.018	0.020	2 4.0	W
KW222	10.328305	40.602414	20.129	0.449	0.846	0.564	0.755	0.018	0.053	0.047	0.028	0.029	2 4.4	W
KW223	10.329911	40.751170	18.912	0.245	0.967	0.585	0.696	0.016	0.019	0.021	0.023	0.020	2 3.4	...
KW224	10.335542	40.607217	20.567	-0.324	0.059	0.080	0.004	0.021	0.023	0.027	0.035	0.064	2 3.0	W
KW225	10.337147	40.984619	18.108	0.600	1.185	0.685	0.764	0.011	0.021	0.016	0.015	0.019	2 3.4	...
KW226	10.337538	40.737319	20.156	0.201	0.530	0.436	0.632	0.016	0.026	0.026	0.026	0.027	2 3.0	...
KW227	10.337729	40.703663	19.922	0.163	0.597	0.396	0.619	0.018	0.024	0.024	0.025	0.026	2 3.0	...
KW228	10.340206	40.684549	19.515	-0.049	0.472	0.348	0.427	0.017	0.023	0.023	0.022	0.024	2 3.0	...
KW229	10.342502	40.832947	20.421	0.399	1.051	0.660	0.831	0.017	0.031	0.028	0.024	0.026	3 3.0	...
KW230	10.346623	40.737447	20.572	0.182	0.453	0.317	0.388	0.028	0.034	0.038	0.042	0.050	2 3.0	...

Table 2—Continued

ID ^a	$\alpha_{\text{J}2000}$	$\delta_{\text{J}2000}$	V^{b}	$U-B$	$B-V$	$V-R$	$R-I$	σ_V	σ_{U-B}	σ_{B-V}	σ_{V-R}	σ_{R-I}	$n^{\text{c}} \text{Ap}^{\text{d}} HST^{\text{e}}$	CrossID ^f
KW231	10.347251	40.632507	20.457	0.156	0.423	0.340	0.506	0.025	0.031	0.032	0.035	0.049	2 3.0	A 2:135
KW232	10.350351	40.613058	18.689	-0.217	0.143	0.139	0.224	0.016	0.020	0.023	0.020	0.034	2 4.0	W 1:B342, 3:C44
KW233	10.353653	40.755618	20.091	0.324	0.707	0.404	0.450	0.017	0.029	0.028	0.025	0.031	2 3.0	... 1:SK027A
KW234	10.354185	40.879399	20.617	0.322	0.849	0.482	0.527	0.021	0.032	0.032	0.032	0.039	3 3.0	W ...
KW235	10.355823	40.514885	20.292	0.446	1.705	0.870	0.897	0.024	0.048	0.039	0.032	0.030	1 3.4	... 1:SK078B
KW236	10.358149	40.560832	20.491	0.163	0.438	0.322	0.475	0.021	0.027	0.030	0.035	0.038	2 3.0
KW237	10.358338	40.588542	18.060	0.280	0.904	0.484	0.560	0.011	0.020	0.019	0.015	0.015	2 4.0	... 1:B203D
KW238	10.360732	40.575055	19.364	-1.056	-0.144	-0.019	-0.114	0.017	0.020	0.021	0.024	0.030	2 3.0
KW239	10.362036	40.785281	20.471	-0.331	0.729	0.668	0.902	0.032	0.031	0.041	0.037	0.033	3 3.0	... 1:SK079B
KW240	10.362442	40.693716	19.216	-0.054	0.434	0.338	0.446	0.013	0.029	0.026	0.021	0.030	2 3.0	... 1:SK080B, 3:C45
KW241	10.363461	40.782934	20.284	0.189	0.345	0.255	0.451	0.026	0.032	0.034	0.039	0.048	3 3.4
KW242	10.365117	40.803639	20.154	0.136	0.520	0.571	1.156	0.020	0.027	0.028	0.030	0.028	3 3.0
KW243	10.365311	40.676269	20.014	0.124	0.554	0.330	0.362	0.016	0.023	0.023	0.026	0.041	2 3.2
KW244	10.367149	40.897206	15.498	0.392	0.946	0.571	99.999	0.010	0.014	0.014	0.014	99.999	3 8.0	... 1:B034
KW245	10.372803	40.754689	19.732	0.157	0.396	0.278	0.452	0.015	0.024	0.024	0.025	0.030	2 3.0	... 1:DAO47
KW246	10.373172	40.832824	20.499	0.377	0.992	0.708	0.994	0.021	0.037	0.035	0.028	0.024	3 3.0
KW247	10.374923	40.640602	20.178	-0.263	0.258	0.287	0.557	0.017	0.024	0.023	0.027	0.035	2 3.0
KW248	10.376253	40.809082	20.448	0.192	0.209	0.090	0.099	0.022	0.032	0.034	0.041	0.066	3 3.0
KW249	10.378169	40.966970	19.136	0.292	1.434	0.780	0.950	0.014	0.028	0.024	0.019	0.019	2 5.0	W ...
KW250	10.378823	40.652302	20.254	0.215	0.760	0.478	0.623	0.017	0.034	0.031	0.024	0.030	2 3.0	... 1:SK098C
KW251	10.379814	40.770182	19.463	0.155	0.305	0.209	0.262	0.013	0.022	0.019	0.023	0.028	3 3.0
KW252	10.382167	40.670940	20.522	-0.020	0.766	0.555	0.782	0.021	0.031	0.031	0.031	0.029	2 3.4
KW253	10.382816	40.748459	20.512	0.112	0.245	0.140	0.339	0.021	0.027	0.030	0.038	0.062	2 3.0
KW254	10.385014	40.817908	20.298	0.250	0.778	0.476	0.468	0.019	0.031	0.029	0.029	0.034	3 3.4
KW255	10.386049	40.790661	20.508	0.244	0.505	0.369	0.675	0.021	0.040	0.040	0.032	0.037	3 3.4
KW256	10.387682	40.656600	20.300	-0.131	0.366	0.286	0.586	0.020	0.026	0.029	0.033	0.037	2 3.0
KW257	10.388505	40.745833	20.572	0.268	0.686	0.504	0.752	0.027	0.042	0.041	0.040	0.042	2 3.0
KW258	10.389102	40.922379	20.481	0.247	1.525	0.917	1.010	0.023	0.069	0.066	0.028	0.023	2 3.2
KW259	10.389519	40.662337	20.295	0.106	0.330	0.180	0.140	0.019	0.027	0.028	0.033	0.047	2 3.0
KW260	10.389539	40.619104	19.726	-0.013	0.231	0.179	0.229	0.013	0.019	0.020	0.020	0.028	2 3.0
KW261	10.389918	40.821267	20.533	0.051	1.351	0.756	0.821	0.026	0.068	0.049	0.035	0.034	3 3.6
KW262	10.391737	40.638352	20.241	0.179	0.421	0.238	0.266	0.019	0.029	0.027	0.029	0.038	2 3.4
KW263	10.391747	40.706410	20.203	0.356	0.887	0.572	0.816	0.016	0.034	0.029	0.032	0.046	2 3.0	... 1:SK030A
KW264	10.393275	40.870829	19.964	0.159	0.425	0.353	0.519	0.017	0.030	0.028	0.034	0.038	3 3.0
KW265	10.394927	40.873771	20.131	-0.110	0.623	0.531	0.690	0.019	0.028	0.027	0.027	0.029	3 3.0
KW266	10.395846	40.763424	19.814	0.220	0.677	0.425	0.507	0.015	0.023	0.022	0.022	0.041	2 3.0
KW267	10.398285	40.927451	19.739	0.430	1.859	0.831	0.839	0.015	0.039	0.029	0.023	0.025	2 3.0	W ...
KW268	10.398552	40.971065	20.399	0.118	0.765	0.517	0.546	0.022	0.033	0.034	0.032	0.036	2 3.0
KW269	10.399226	40.583480	20.532	-0.144	1.057	0.631	0.882	0.017	0.034	0.031	0.023	0.024	2 3.0
KW270	10.402374	40.963358	19.779	0.182	0.346	0.234	0.345	0.015	0.020	0.021	0.026	0.035	2 3.0
KW271	10.403081	40.789778	19.021	0.133	0.902	0.578	0.736	0.012	0.020	0.018	0.017	0.026	3 3.0	... 1:G099
KW272	10.403145	40.846700	20.266	0.398	1.219	0.797	0.975	0.021	0.048	0.037	0.028	0.024	3 3.0
KW273	10.403635	40.790430	18.731	0.191	0.470	0.332	0.415	0.013	0.018	0.019	0.018	0.019	3 3.0	... 1:G099, 3:C46
KW274	10.404677	40.946935	20.517	0.412	1.373	0.651	0.633	0.027	0.059	0.055	0.038	0.045	2 3.4
KW275	10.405306	40.680437	20.142	0.212	0.468	0.293	0.366	0.016	0.032	0.026	0.026	0.029	2 3.0
KW276	10.405555	40.889606	20.440	-0.013	0.272	0.217	0.305	0.022	0.025	0.029	0.035	0.046	3 3.0	W ...

Table 2—Continued

ID ^a	$\alpha_{\text{J}2000}$	$\delta_{\text{J}2000}$	V^{b}	$U-B$	$B-V$	$V-R$	$R-I$	σ_V	σ_{U-B}	σ_{B-V}	σ_{V-R}	σ_{R-I}	n^{c}	Ap ^d	HST^{e}	CrossID ^f
KW277	10.406892	40.810644	20.359	0.350	0.872	0.599	0.848	0.020	0.039	0.036	0.027	0.028	3	3.6
KW278	10.408178	40.794982	19.757	0.261	0.516	0.393	0.589	0.018	0.034	0.027	0.029	0.030	3	3.0
KW279	10.408569	40.569612	18.947	-0.257	0.612	0.392	0.599	0.011	0.028	0.017	0.021	0.024	2	3.0	...	1:B205D, 3:C47
KW280	10.410253	40.974239	19.647	0.356	0.823	0.447	0.440	0.026	0.031	0.035	0.044	0.044	2	3.6	...	1:SK032A
KW281	10.410497	40.826785	19.296	0.287	0.509	0.329	0.357	0.014	0.023	0.019	0.019	0.020	3	3.0	A	3:C48
KW282	10.411205	40.733145	18.791	-1.144	0.022	0.502	-0.385	0.012	0.031	0.020	0.016	0.021	2	3.6	...	1:SK083B, 3:E52
KW283	10.411669	40.799712	20.229	0.486	1.439	0.746	0.877	0.018	0.047	0.034	0.025	0.026	3	3.6	A	...
KW284	10.411797	40.681812	18.111	-0.213	0.270	0.239	0.307	0.011	0.032	0.019	0.015	0.015	2	3.0	...	1:B040, 3:C49
KW285	10.415594	40.942668	19.605	0.368	1.651	0.744	0.809	0.015	0.033	0.028	0.023	0.025	2	3.6	...	1:SK099C

Note. — R.A. and Decl. (J2000) coordinates of aperture centers are in the USNO-B1.0 catalogue system (degrees). An entry “99.999” is for $R-I$ and σ_{R-I} of 5 objects saturated in the I -band images.

^aID number of the star cluster candidate.

^bAperture magnitude (note, it is not a total magnitude).

^cNumber of independent measurements in the LGGS fields F6–F9.

^dDiameter of circular aperture or major axis length of elliptical aperture (arc-seconds). Elliptical apertures (ratio of minor to major axis; position angle of the major axis, calculated counterclockwise from the North direction) are used for objects KW102 (0.75; 120°) and KW141 (0.70; 30°).

^eIdentification of 77 objects in the HST instrument frames: W – WFPC2 (71), A – ACS (6).

^fCross identifications “catalog:id”. (1) – The Revised Bologna Catalogue of M31 globular clusters and candidates v.3.2, July 2007 (Galletti et al. 2007) – 69 objects. KW128 is identified with V203 and KW129 – with V202, however, coordinates are offset; KW271 and KW273 are identified as one object – G099. (2) – Krienke & Hodge (2007) “KHM31” numbers are given only for 24 objects not listed in (1). KW154 has two identifications: KHM31-79 and KHM31-80. (3) – Kodaira et al. (2004) “KWC” and “KWE” numbers are given for 58 objects. KW063 is identified with KWE09 and KW095 – with KWE19, however, center coordinates and apertures are slightly different.

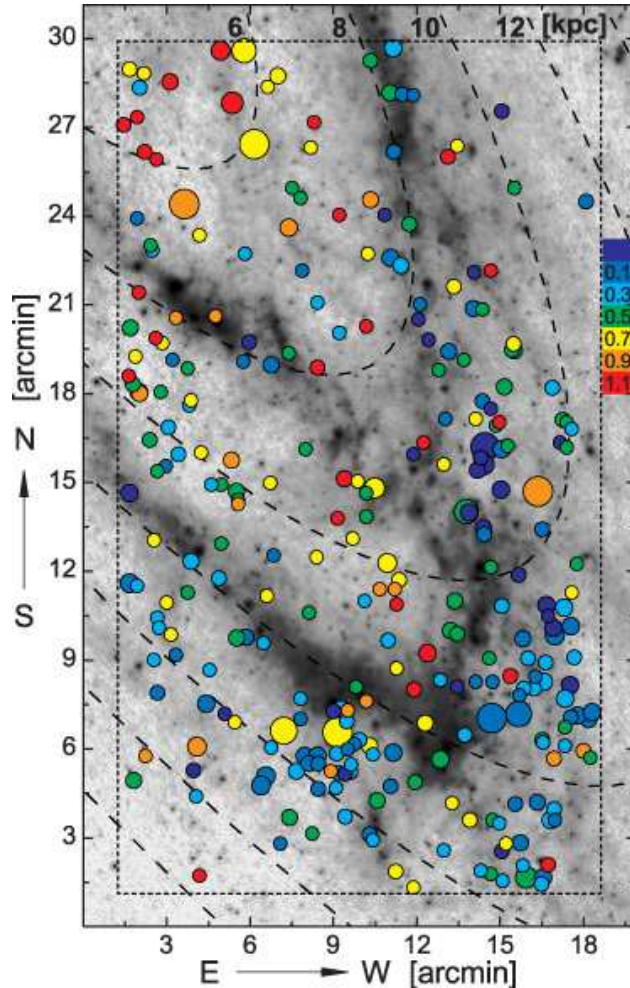


Fig. 1.— Star cluster candidates (285 objects) in the M31 SW field are overlaid on the *Spitzer* (24 μ m) image. Circle size corresponds to the V-band magnitude, and circle color represents the observed $B-V$ (see the color bar for coding). Elliptical ring segments, indicating distances from the M31 center (6 – 18 kpc), are marked with dashed lines. The rectangle (dotted line) indicates the Suprime-Cam survey area. North is up, east is left.

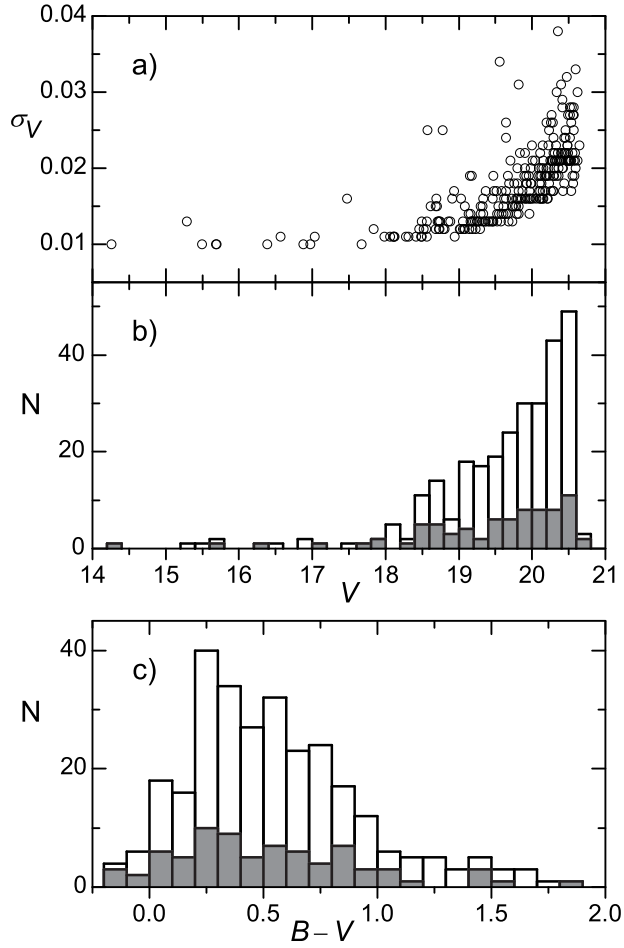


Fig. 2.— Global characteristics of the star cluster candidate catalog (285 objects). Panels show (a) the photometric errors, σ_V , vs. V -band magnitudes (we adopted the lowest possible error of $\sigma_V = 0.01$ mag); (b) the observed V -band magnitude histogram (an object selection criterion is $V \lesssim 20.5$ mag); (c) the observed $B-V$ color histogram. Gray-shaded histograms are constructed for a sub-sample of 77 objects, located in the *HST* frames.

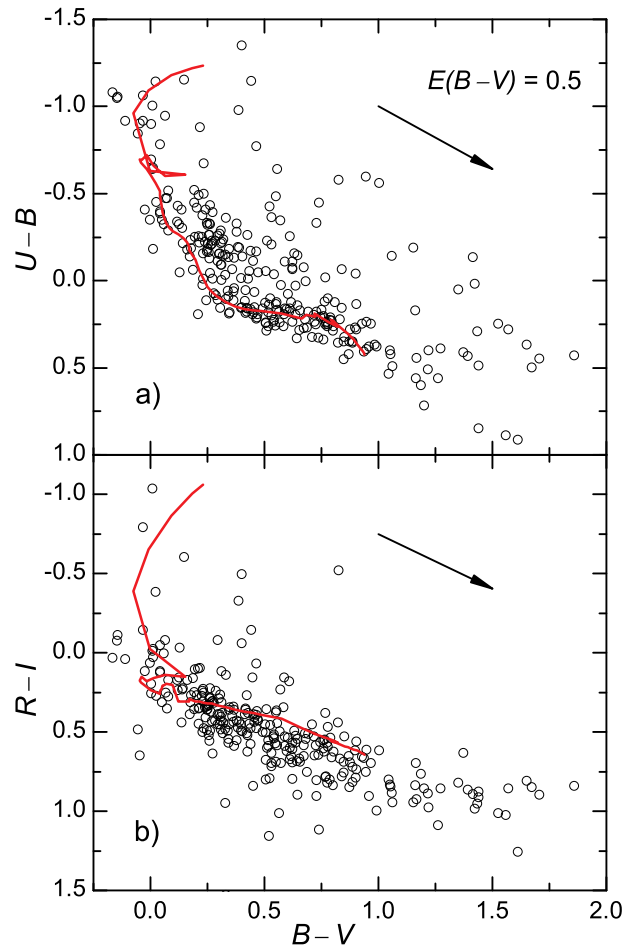


Fig. 3.— Observed color-color diagrams of 285 catalog objects (*circles*). PÉGASE SSP models of $Z = 0.008$ and ages ranging from 1 Myr to 15 Gyr are marked with solid lines. The reddening vectors of $E(B-V) = 0.5$, corresponding to the standard extinction law, are indicated.

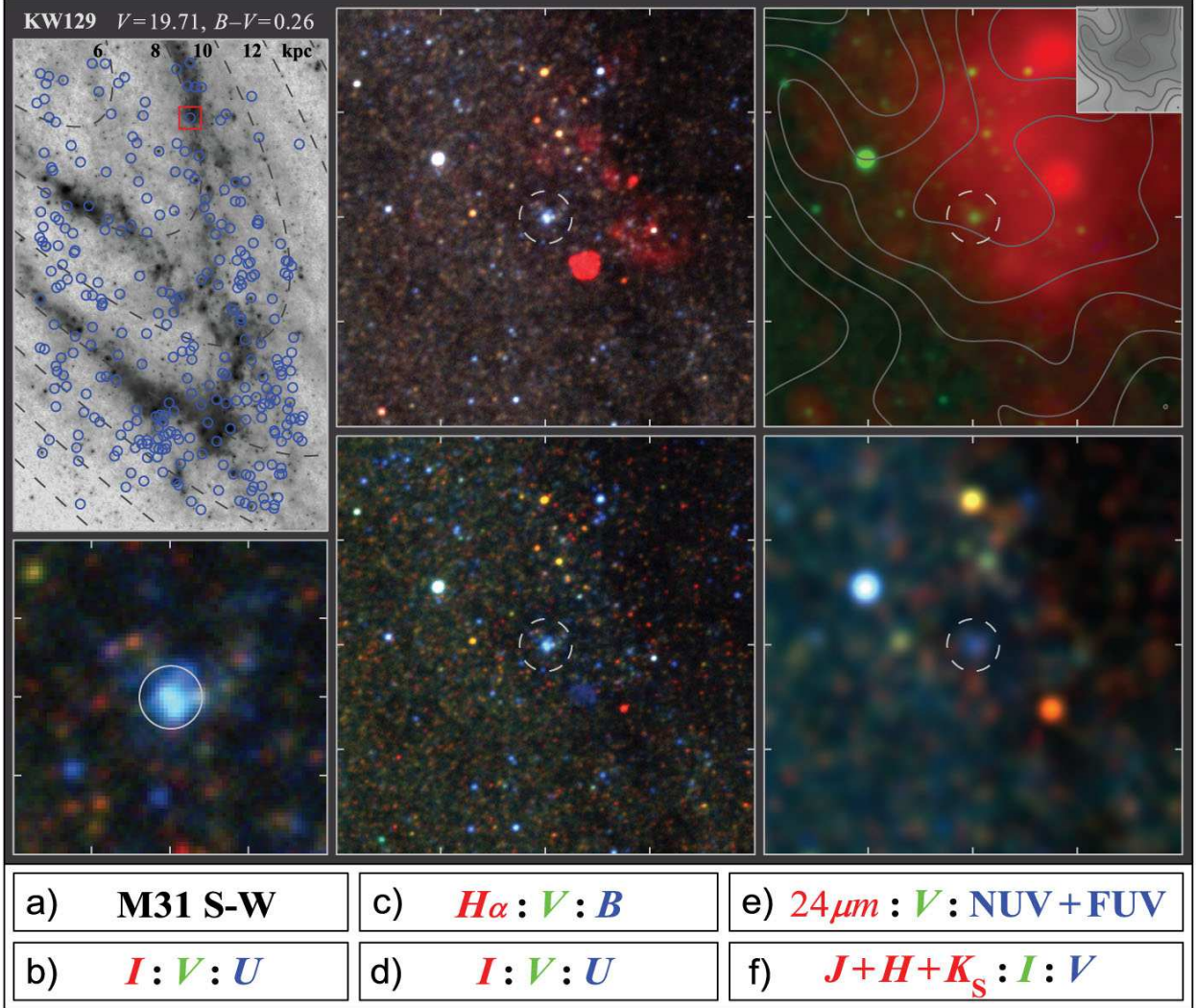


Fig. 4.— An example of multiband maps (*top*) and a corresponding layout template (*bottom*), indicating panel notations, is shown here as a guide to the individual multiband color maps, constructed for all objects, available in the electronic edition of the *Supplement*. The object’s ID, the V -band magnitude, and the $B-V$ color are provided in the top-left corner. Panel *a* shows positions of 285 objects in the M31 SW field (*circles*); elliptical ring segments indicating distances from the M31 center (6 – 18 kpc) are marked with dashed lines overlaid on the *Spitzer* ($24\mu\text{m}$) image; the object under consideration is indicated by a red square of a size equivalent to the size of panels *c-f*. In panels *b-f* of the layout template, passbands of images displayed in red, green, and blue color channels are indicated by corresponding colors. The LGGS images were used in panels as follows: (*b-d*) U , B , V , I , $H\alpha$ bands of the original resolution; (*e*) the V -band of a homogenized PSF ($\text{FWHM} = 1.5''$); (*f*) the V and I bands of a homogenized PSF ($\text{FWHM} = 3.5''$) matching the PSF of 2MASS images. Contour lines in panel *e*) emphasize the HI distribution; the gray-shaded inset shows a global 21 cm emission intensity, black standing for the highest and white for the lowest signal level over the entire surveyed area. The size of panel *b* is $15'' \times 15''$, and the size of panels *c-f* is $80'' \times 80''$. The aperture used for the photometry is overlaid in panel *b*. The object in panels *c-f* is marked with a circle of $10''$ in diameter. North is up, east is left. [See the electronic edition of the *Supplement* for figures 4.1 – 4.285.]